Design Optimisation of High Performance Fractional-slot Distributed Winding PM Synchronous Machines for In-wheel Application in Electric Vehicles

S.Bandyopadhyay, Martin van der Geest, Henk Polinder

Delft University of Technology, The Netherlands, s.bandyopadhyay@tudelft.nl

Keywords: Electromagnetic Torque, Finite Element Method (FEM), Fractional-Slot distributed winding, Multi-Objective Optimisation, Particle Swarm Optimization, PM machines, Torque ripple.

Abstract

In general, PM machines with conventional integer slot distributed winding (ISDW) schemes exhibit significant cogging torque resulting in high torque ripple which makes them unsuitable for EV applications which require low torque pulsations. This paper presents detailed analysis of the performance of PM Synchronous motor (PMSM) with fractional slot distributed winding (FSDW) scheme which shows significant reduction in torque ripple compared ISDW PM machines. Effect of the fractional slot winding distribution on electromagnetic torque pulsations has been analysed using Finite element (FE) computation technique. For a fair quantitative comparison between the above machine types, a flexible optimisation approach is proposed in this paper which generates Pareto fronts of the individual machine types.

1. Introduction

Surface-mounted PM synchronous motors (PMSMs) are widely used in Electric Vehicle applications for their high efficiency, compact and simple mechanical construction and good dynamic torque response [1].

One of the major problems in PMSM is the torque ripple which is inherent in their design. This ripple is parasitic, and can lead to mechanical vibration, acoustic noise, and reduces ride comfortability. Minimizing this ripple is of great importance in the design of PMSMs [2].

Torque ripple in PM machines has mainly two sources [3–5]: a) Cogging Torque, b) Airgap magnetic flux density distortion. Cogging torque results from the interaction of permanent magnet field and stator slot openings and it is normally independent of any excitation in the stator windings. Extensive research on reduction of cogging torque in PMSM can be widely found in literature [6]. The cogging torque characteristics depend mainly on the combination of slot and pole number and is inversely proportional to the lowest common multiple of number of slots (Q_s) and number of poles ($2P$) [6,7].

Integer slot distributed winding PM machines have the highest fundamental winding factor (k_w = 1) among all winding families. Therefore, it has high electromagnetic torque per ampere capability [8]. In addition to that, their winding MMF spectrum has very low harmonic content which leads to low rotor eddy current losses. However ISDW PM machines suffer from a major drawback of having inherently high cogging torque owing to low values of LCM (Q_s,$2P$), as their slot/pole/phase (q) is always an integer [9].

To mitigate the high torque ripple problem in conventional ISDW machines, fractional slot concentrated winding(FSCW) schemes with $q \leq 0.5$ have been proposed widely in literature [2,3]. Some winding schemes in this winding family show very low torque ripple. In addition to that, they have shorter end windings which leads to reduced copper weight and copper losses leading to high efficiency and torque density. However, their winding MMF distribution have relatively high space harmonic and sub-harmonic content which can induce high magnet and rotor losses. Also FSCW machines have high pole numbers which lead to high electrical frequencies, thus resulting in high iron losses [10].

This paper aims to demonstrate an unconventional fractional slot distributed winding scheme as an alternative design strategy to combine the best of both ISDW and FSCW PM machines in terms of high torque capability, low torque ripple and relatively low total harmonic distortion (THD) in three phase MMF spectrum. The proposed winding scheme has 87 slots and 28 poles whose overall layout is quite close to conventional ISDW PM machine with 84 slots/ 28 poles. The windings strategy of the aforementioned scheme is briefly discussed to highlight the deviations from conventional winding schemes. A comparison between the above machine types is only fair if they are optimally designed for similar scenarios. For that purpose, next the paper focuses on design optimisation of PM machines with the proposed winding scheme to check their comparative suitability with conventional ISDW winding PM machines for EV application over a wide design range.

Nowadays with increased computer speeds, Finite Element (FE) machine models are combined with optimisation algorithms to design high performance electric machines for a wide range of applications including Electric Vehicles [11]. Design optimisation of PM machines with FSCW and ISDW schemes are widely reported in literature [12]. Due to their winding symmetry, the computation time for design optimisation is significantly reduced. However, for the proposed winding scheme, design optimisation is hindered by their asymmetric winding distribution. To tackle this problem the paper presents a novel methodology of optimising machine designs with asymmetric winding schemes similar to the prposed

87/28 machine. Multi-objective PSO algorithm is used to optimize the machines which generates Pareto optimal fronts [13]. These fronts are further analysed to compare the holistic performance of the machines with integer slot and fractional slot distributed winding winding schemes [14].

2. Winding Analysis

The winding layout and analysis of the proposed winding scheme with 87 slots/ 28 poles is based on the voltage phasor method, which is also known as star of slots method in literature [15,16]. Detailed analysis of winding design using voltage phasor or star of slots method is not in the scope of this paper. Therefore some key parameters and rules are presented for basic understanding.

2.1 Winding Layout and Slot-star diagram

The star of slots is the phasor representation of the main EMF harmonic induced in the coil side of each slot. The relevant parameters of the slot-star diagram used for determination of the winding layout are presented in Table 1. The star of slots

Table 1. Winding parameters of fractional slot windings.

Parameter	Symbol	Equation
Machine Periodicity	t	$t = gcd\{Q, p\}$
Slots/pole/phase	q	$q = \frac{z}{n} = \frac{Q}{2pm}$
Number of radii	Q'	$\frac{Q}{t}$
Pole pairs in base winding	p*	$\frac{n}{2}$
Slot angle	α_u	$\alpha_u = 360^o \times \frac{p*}{Q}$
Phasor Angle	α_z	$\alpha_z = 360^o \times \frac{t}{Q}$
Number of Phasors skipped in numbering	Z	$\frac{p*}{t} - 1$

EMF phasor diagram of the 87/28 winding scheme is shown in Figure 1. The winding layout is derived from the slot star diagram. Once the winding layout is determined, the winding factor can be computed for any harmonic.
To get a fair idea about the difference between the proposed winding scheme of 87 slot 28 pole machine and a conventional integer slot distributed winding, a comparative winding study with an ISDW with 84 slots 28 poles is presented in Table 2.
The fundamental winding factor of the 87 slot 28 pole machine

Table 2. Comparison of winding data of fractional slot 87/28 machine with integer slot 84/28 machine .

Winding Parameters	84/28 machine	87/28 machine
Number of slots	84	87
Number of Poles	28	28
Slot/pole/phase	1	1.0357
Winding Layers	1	2
Winding Pitch	3	3
Winding factor (k_w)	1	0.954

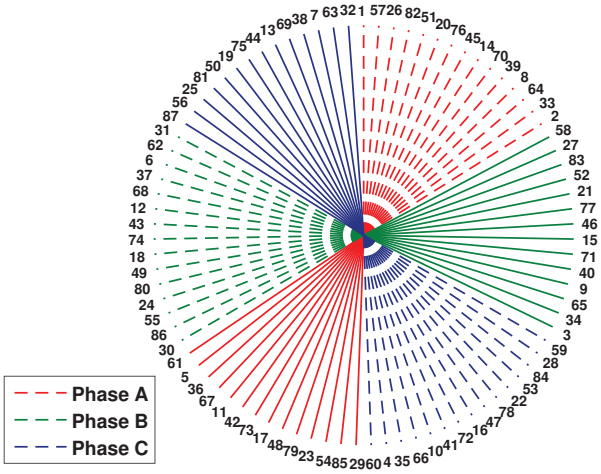

Figure 1. Star of slots phasor diagram of 3 phase double layer winding Q = 87, p = 14, t = 1, n = 28, p* = 14, $\alpha_u = 14\alpha_z = 57\frac{27}{29}^o$, $\alpha_z = 4\frac{4}{29}^o$, Z = 13. Phasors belonging to positive phases are illustrated by solid lines.

is a bit lower than the conventional integer slot 84 slot 28 pole machine, which means reduced electromagnetic torque capability of PM machines with 87/28 combination. However, least common multiple (LCM) of the 87 slot 28 pole machine is significantly higher than its integer slot counterpart which suggest a reduction in cogging torque or torque ripple.

2.2 Harmonic Analysis

FFT analysis of the 3-phase airgap-MMF distribution of the integer slot winding scheme and the fractional slot winding scheme is carried out to extract the harmonic spectrum. Figure 2 shows the harmonic content of the two winding distributions.
As expected, the winding spectrum of the integer slot is clean with presence of some 5th, 7th, 11th and 13th order multiples of the working harmonic pole pairs (14). However, the major difference can be seen in the presence of significant subharmonics which may lead to increased eddy losses in rotor magnets.

3. Machine analysis and Optimisation

In this section, the machine modelling framework is briefly discussed. Initially, the FE modelling procedure to compute the electromagnetic performance of the machine is highlighted. To gain insights into the holistic thermo-electromagnetic performance of the machine a circuit thermal model (combined with FE electromagnetic model) of the PM machine is built. The thermal model uses the losses predicted by the electromagnetic model to simulate the thermal behaviour of the machine.

3.1 Machine Analysis

The numerical machine analysis is performed by a combination of MATLAB to create and postprocess the FE models and

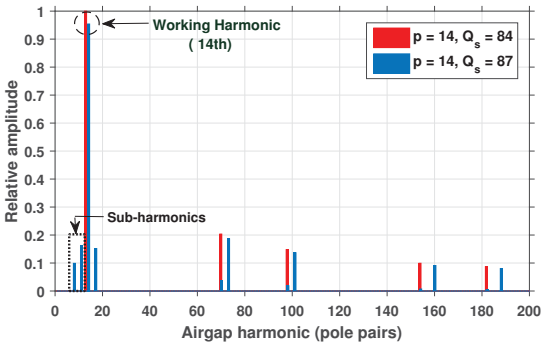

Figure 2. Harmonic spectrum of three phase airgap MMF distribution of integer slot 84/28 winding (red) and fractional slot 87/28 winding (blue),showing the presence of 5th, 7th, 11th and 13th harmonics of individual mmf spectrum. MMF spectrum of 87/28 winding shows presence of sub-harmonics which may lead to increase of rotor eddy losses

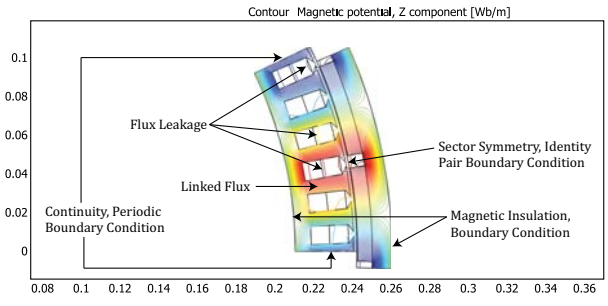

Figure 3. Finite Element Model of a symmetrical integer slot 84 slot 28 pole machine with sector symmetry ($n_{sector} = 14$) and continuity boundary conditions. Contour plot of magnetic vector potential A_z showing the distribution of flux linkage and different kinds of leakage fluxes in a machine model

COMSOL to solve the FE models. To save time a computationally efficient FE machine model is created exploiting the winding symmetry of an integer slot PM machine. The field distribution of a full geometry 84/28 PM machine can be computed by solving on the fraction containing 6 slots and 2 poles and using periodic boundary conditions and sector symmetry as explained in Figure 3. To save time a minimum number of preferably static simulations is executed and the machine characteristics are obtained by post processing the results [14]. The analysis of a single machine is comprised of the following steps:

- Compute flux linkage, back-emf waveforms and the d-axis offset from static simulations.
- Compute the inductances using change of linked flux method [17] to include effect of core saturation.
- Computation of torque characteristics using filtered Maxwell stress tensor method [18]. Non-linear FE models are used to take effect of core saturation.
- Computation of copper, iron and magnet weights.
- Computation of slot copper losses and iron losses. The latter are computed by using manufacturer data combined with the AC flux density to compute the loss density throughout the entire stator, thereby correctly taking local high flux densities into account as shown in figure 4.
- Computation of overall electrical efficiency at a certain operating point.
- Computation of steady state machine temperatures using lumped circuit parameter thermal model [19] as shown in Figure 5.
- Compute boost torque capability at maximum inverter current to check core saturation effects on boost operation.

3.2 Particle Swarm Optimisation

The optimization algorithm used is particle swarm optimization, an evolutionary gradient free method based on the movement of birds or insects in a swarm. This algorithm was selected because it is gradient free and potentially requires very few function calls [20].

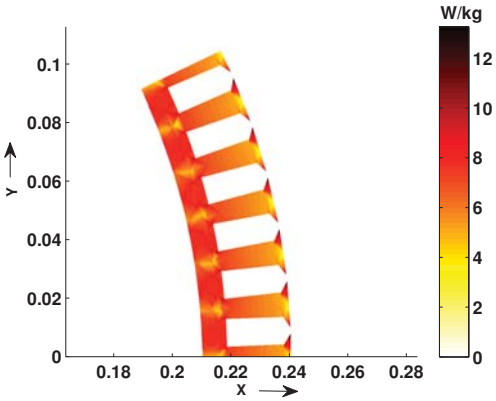

Figure 4. Example of stator lamination loss density distribution (W/kg)

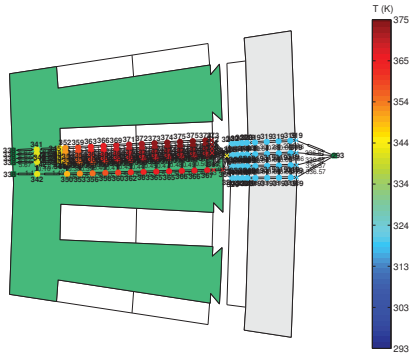

Figure 5. Example of steady state node temperature distribution of a 84/28 slot machine design at a certain continuous operating point of torque and speed using circuit thermal model. Assuming symmetry, only half a slot and half a tooth thermal behaviour is simulated. As expected, thermal hotspots are mostly concentrated in copper slots.

1) Multi-Objective PSO: A modified version of the original algorithm is used here to work with multiple targets simultaneously, which allows the pareto optimal fronts [13] to be computed. This is accomplished by storing all pareto optimal solutions in a repository and picking the global best target ran-

domly from this repository.
2) Solution Space and Constraint handling: To prevent unnecessary exploration of uninteresting design regions and save computing time, the global targets are confined to more promising parts of the solution space, such as high efficiency or low weight designs. To ensure variable values within constraints, velocity reduction techniques on particles are used.

3.3 Optimisation Targets, Variables, Constraints

The setup of the optimization consists of specifying variables, constants (including material properties), constraints and targets. Figure 6 shows the variables and Table 3 presents the range of the variables. Table 4 presents the assumed material properties of the PM machine.
Considering a theoretical 60 kW rated 400 rpm PM motor for in-wheel EV application, the following global optimisation targets are chosen:

- Minimize active machine weight
- Maximize electrical efficiency at continuous operating point
- Maximize peak torque capability

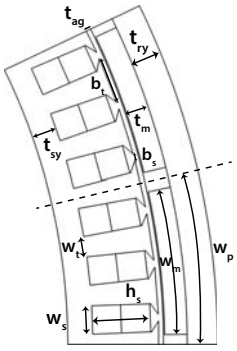

Figure 6. Graphical representation of optimisation variables. In addition, the machine stack length (L) and outer rotor radius (D_{or}) are also variables of optimisation.

Table 3. Design variable and their ranges. Magnet Span (α_m) is defined as $\frac{w_m}{w_p}\%$, $k_{open} = \frac{b_s}{b_s+b_t}$, $\alpha_{slot} = \frac{w_s}{w_s+w_t}\%$.

Variables	Symbol	Range
Rotor Diameter(m)	D_{or}	$D_{or} \leq 0.275$
Rotor yoke thickness(mm)	t_{ry}	$10 \leq t_{ry} \leq 30$
Airgap thickness (mm)	t_{ag}	$1.5 \leq t_{ag} \leq 3$
Magnet thickness (mm)	t_m	$3 \leq t_m \leq 8$
Magnet Span(%)	α_m	$40 \leq \alpha_m \leq 96$
Stator Slot opening relative	k_{open}	$0.25 \leq k_{open}$
Slot height (mm)	h_s	$20 \leq h_s \leq 50$
Slot base span (%)	α_{slot}	$40 \leq \alpha_{slot} \leq 60$
Stator yoke thickness (mm)	t_{sy}	$5 \leq t_{sy} \leq 20$
Machine Stack length(m)	L	$L \leq 0.3$

Table 4. Assumed Material Properties.

Magnets	N-38H B_r = 1.2 T μ_r = 1.05
Stator Iron	non-linear: M350-50
Rotor Iron	non-linear: ST-37
Fill factor	40 %

3.4 Optimisation Methodology

As already discussed in Section 3.1, to make the machine models computationally efficient, winding symmetry is exploited using sector symmetry boundary conditions. However, this approach is only applicable to symmetrical windings like integer-slot winding like 84 slot/ 28 poles scheme. The proposed winding scheme with 87 slot-28 poles is devoid of any such winding symmetry which forces the designer to use only full scale FE models which increases the computational load and solution time as highlighted in Table 5. The PSO algorithm used here, solved for 20 particles per iteration with a minimum of 100 iterations. That means analysis of minimum 2000 machine designs. This effectively rules out optimising the 87/28 machine which will take months to reach optimal designs. To get around this problem, a methodology of optimising asymmetrical winding machine designs has been proposed. The method is presented here and the results obtained are analysed in the next section.

Table 5. Comparative study of finite element computational details of integer slot machine and fractional slot machine.

	84/28 machine	**87/28 machine**
Base Winding	6/2	87/28
Symmetrical Sectors	14	1
Degrees of freedom (DOF)	8 - 10 k	150 -200 k
Computation Time (mins)	2-3	40-55

The methodology has been presented in the following steps:

(1) Select a symmetrical machine which is closest to the original asymmetrical one in terms of winding characteristics and slot/pole combination. In this case it will be a machine with 84 slots /28 poles.
(2) Exploiting the symmetry of the machine optimise the design with the same optimisation targets, settings, variables and constraints which are originally intended for the asymmetrical winding machine.
(3) Generate pareto fronts of the optimisation targets and select randomly a bunch of optimal particles or designs.
(4) Make modifications on the selected optimal designs of the symmetrical machine to create designs of the asymmetrical machine.
(5) Analyse the modified asymmetrical designs using Finite element models and extract all the relevant performance data.
(6) Plot the performance data of the asymmetrical machines and compare their positions with respect to the pareto front of the optimal symmetrical designs.

(7) If the positional deviations of the 87/28 machine designs are consistent with respect to the pareto front of the symmetrical 84/28 machines, it can concluded with reasonable certainty that the asymmetrical machine designs represent a pareto front of their own.

3.5 Optimisation Results

The resulting pareto fronts are shown in Figure 7 and Figure 8. The front is represented by approximately 250 particles or optimal designs. Out of these, 45 designs are chosen randomly (highlighted in red) for further analysis of the asymmetrical 87/28 machine. The steps to convert the 84/28 design to a 87/28 design are presented below:

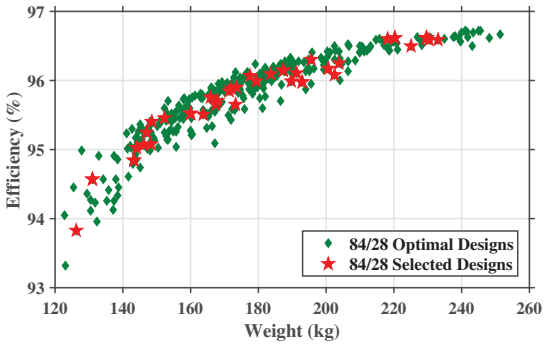

Figure 7. Maximum Efficiency versus machine active weight. The trend shows increasing efficiency with heavier machine designs due to operation at lower flux densities and current densities leading to lower losses and higher efficiencies.

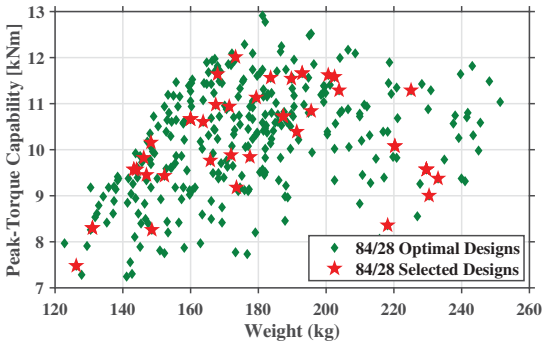

Figure 8. Boost torque versus machine active weight.

- The rotor geometry remains same since both the designs have the same number of poles.
- The radial stator dimensions like outer radius (D_{or}),inner radius, slot height (h_s) and stator-rotor yoke thickness (t_{sy}, t_{ry}) also remains same.
- Tangential relative dimensions like relative slot opening (k_{open}), slot base span (α_{slot}) are kept constant. Therefore absolute tangential dimensions like tooth width (b_t), absolute slot opening width (b_s), slot width (w_t) are modified to fit the 3 extra slots. See Figure 6 for reference.

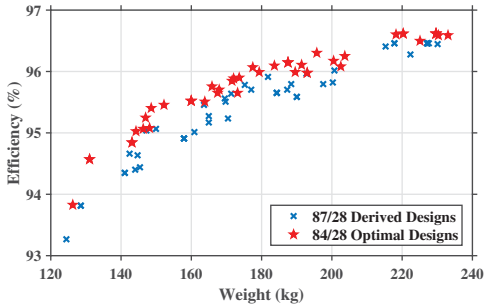

Figure 9. Comparison of efficiency of derived 87/28 machines with optimal 84/28 machines. The trend of lower efficiency in the derived designs seems consistent. Increased copper losses due to lower winding factor leading to higher required current for same operating torque

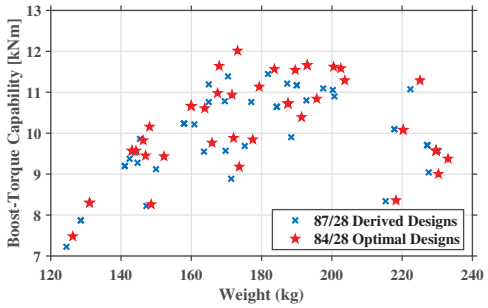

Figure 10. Comparison of boost torque capabilities shows reduction in capabilities mainly due to reduced winding factor of the 87/28 machine

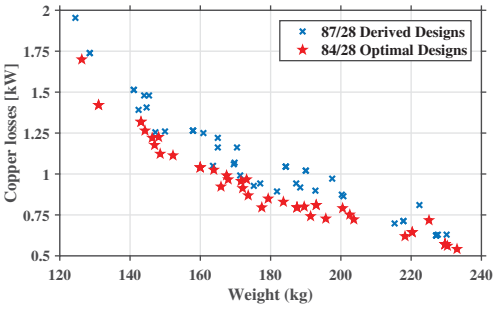

Figure 11. Comparison of copper losses between derived 87/28 machines and 84/28 machines show increased copper losses in the derived designs. The reasons for increase are twofold, a) Higher current needed to produce same torque due to lower winding factor b) Addition of copper in three extra slots leading to higher phase resistance

- Once the stator geometry with 87 slots is obtained, the winding layout discussed in Section 2. is imposed on the stator.

Once the modified asymmetrical designs are obtained, they are analysed by the FE machine model. Their performance are compared with respect to the optimal integer slot 84/28 machine designs. The comparison of the performances are shown in Figures 9 - 14. The results are briefly discussed in the following:

- Figure 9 shows the plot of the maximum efficiency of the

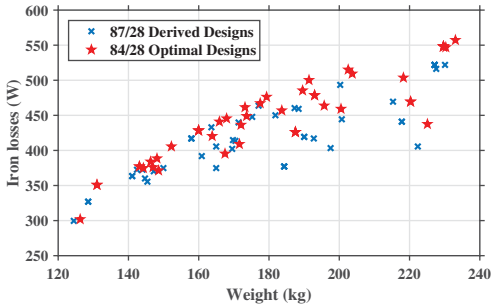

Figure 12. Comparison of iron losses show a small reduction of iron losses in the derived designs. It is mainly due to slightly lower iron weight in the derived 87/28 designs due to extra slots

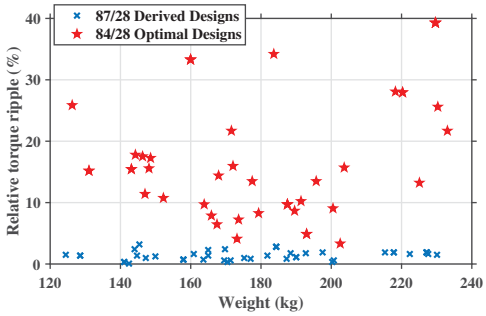

Figure 13. Comparison of on-load torque ripple characteristics reveals significant reduction in the derived 87/28 designs mainly due to high value of least common factor of slots and poles leading to low cogging torque

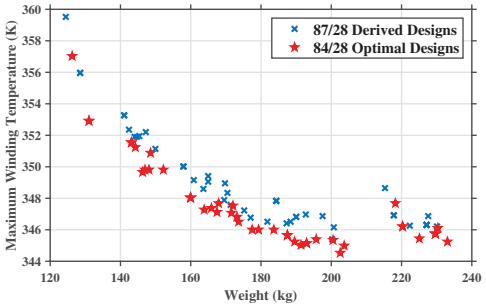

Figure 14. Comparison of maximum temperature in slot-windings showing increase in temperature in the derived 87/28 designs due to increase in copper losses

modified derived 87/28 machines with respect to the Pareto fronts of the optimised 84/28 machines. It can be seen, that the general trend of the derived designs follow that of the optimal designs.

- Figure 10 shows the comparison of the boost torque capability of the derived and optimal designs. In general, the 84/28 designs have slightly higher boost torques which is expected given that it has 5% higher winding factor (k_w) which leads to higher flux linkage for same amount of magnet material, thus capability of producing higher torque for a given current.
- The copper losses at a fixed operating torque is shown in Figure 11 for both the machines. The plots show increase in the copper losses of the modified 87/28 machines. With the increase of linked flux due to high fundamental winding factor, the 84/28 machines need lower current to produce the same torque given by the proportionality, $T_e \propto \lambda I$ where λ is the linked flux and I is the current. With the reduction of required current, the copper losses are also decreasing. In addition to that, the phase resistance of the derived 87/28 machines is higher due to extra copper addition to the three extra slots. This also explains the reduction of the efficiency of the 87/28 machines with respect to the optimal 84/28 machines.
- Figure 12 shows the iron losses of both the machines at a constant operating speed. The plot shows that the 87/28 machine has in general slightly lower iron losses than its 84/28. It is mainly due to slight reduction in total iron weight in the derived 87/28 machines due to presence of extra slots.
- Figure 13 shows the comparison of the relative torque ripple of the 87/28 machines and the 84/28 machines. It can be seen, that the torque ripple has reduced significantly. This characteristics seem to be pretty consistent over the entire range of designs.

Considering the results obtained by applying the proposed methodology, it seems like it can be a very efficient way of design optimisation of asymmetrical fractional slot distributed winding machines like 87/28.

4. Analysis of Pareto Optimal Machines

To obtain an impression of the optimal machine designs, performance parameters of a randomly selected design are highlighted in Table 6. It also shows the main differences in performance and relevant dimensions between the derived 87/28 and the 84/28 machine designs. The deviations of the performance parameters are in line with the explanations discussed in the previous section. The difference in the tangential stator dimensions of the selected machines can also be seen the table.

The torque ripple shape is shown in Figure 15. it is quite clear that 87/28 machine shows very low torque ripple. The machines considered here have six cogging periods per electrical period as can be seen in the Figure.

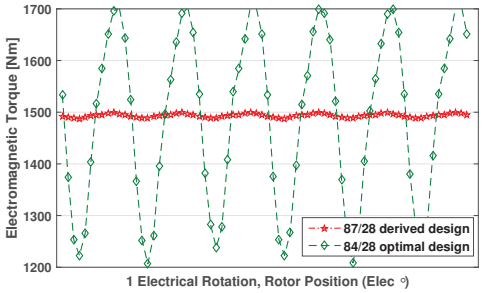

Figure 15. Comparison of on-load torque ripple characteristics over one electrical rotation

Table 6. Parameters of selected optimal machines.

Parameters	84/28	87/28
Efficiency (%)	94.8	94.3
Stator Iron Loss (W)	380	363
Copper Loss (kW)	1.3	1.5
Peak Torque (kNm)	9.5	9.2
Torque Ripple (%)	15.7	0.4
Max.Slot Temperature (^oC)	81	83
Slot-opening Width, b_s (mm)	3.2	3.1
Slot Width, w_t (mm)	9.5	9.2
Tooth Width, b_t (mm)	11	10.8
Slot Height, h_s (mm)	22	22
Copper Weight (kg)	23.2	22.8
Stator weight (kg)	55.5	54.4
Total weight (kg)	133.2	131.3

5. Conclusion

This paper presents a method to optimise fractional slot distributed winding PM machines which are devoid of any winding symmetry using particle swarm optimisation and Finite element analysis for low torque ripple applications like EVs. This method takes into account both electromagnetic and thermal behaviour of machine designs to present an holistic framework of electrical machine designs. To reduce the computational time of design optimisation this paper presents an optimisation strategy using symmetrical winding machines instead.

The method was demonstrated with the optimization of two PM machines for efficiency, weight and peak torque capabilities, but can of course be extended to include other applications and machine types. General trends in the results are found to be in accordance with expectations and shows remarkable torque ripple characteristics of the fractional slot winding machines. The results show that the used approach is suitable for optimisation of fractional slot winding machines. Future work may include in-depth investigation of more fractional slot distributed PM machines and check suitability of the method for designs which are very different from their symmetrical counterparts.

References

[1] J. Wang, X. Yuan, and K. Atallah, "Design Optimization of a Surface-Mounted Permanent-Magnet Motor With Concentrated Windings for Electric Vehicle Applications," *IEEE Transactions on Vehicular Technology*, vol. 62, pp. 1053–1064, Mar. 2013.

[2] J. a. Güemes, a. M. Iraolagoitia, P. Fernández, and M. P. Donsión, "Comparative study of PMSM with integer-slot and fractional-slot windings," *19th International Conference on Electrical Machines, ICEM 2010*, 2010.

[3] U. D. B. Muenchen, D. Neubiberg, A. Ag, and D. Ingolstadt, "Torque Ripple Reduction in Permanent Magnet Synchronous Machines with Concentrated Windings and Pre-Wound Coils," vol. 1, 2014.

[4] R. Islam, I. Husain, A. Fardoun, and K. McLaughlin, "Permanent-Magnet Synchronous Motor Magnet Designs With Skewing for Torque Ripple and Cogging Torque Reduction," *IEEE Transactions on Industry Applications*, vol. 45, no. 1, pp. 152–160, 2009.

[5] H. Dogan, F. Wurtz, A. Foggia, and L. Garbuio, "Analysis of slot-pole combination of fractional-slots PMSM for embedded applications," *International Aegean Conference on Electrical Machines and Power Electronics, ACEMP 2011 and Electromotion 2011 Joint Conference*, pp. 611–615, 2013.

[6] Z. Q. Zhu and D. Howe, "Influence of design parameters on cogging torque in permanent magnet machines," *Energy Conversion, IEEE Transactions on*, vol. 15, no. 4, pp. 407–412, 2000.

[7] Z. Q. Zhu, Z. P. Xia, L. J. Wu, and G. W. Jewell, "Influence of slot and pole number combination on radial force and vibration modes in fractional slot PM brushless machines having single- and double-layer windings," *2009 IEEE Energy Conversion Congress and Exposition, ECCE 2009*, pp. 3443–3450, 2009.

[8] P. H. Nguyen, E. Hoang, M. Gabsi, and M. Lecrivain, "A new method to find the fractional slot windings structures from a distributed slot windings permanent magnet synchronous machine and comparative study for a HEV application," *Proceedings of the IEEE International Conference on Industrial Technology*, pp. 317–322, 2010.

[9] J. A. Guemes, A. M. Iraolagoitia, M. P. Donsion, and P. Fernandez, "Analysis of permanent magnet synchronous motors with integer-slot and fractional-slot windings," in *Melecon 2010 - 2010 15th IEEE Mediterranean Electrotechnical Conference*, pp. 1499–1504, IEEE, 2010.

[10] P. Salminen, M. Niemelä, J. Pyrhönen, and J. Mantere, "High-Torque Low-Torque-Ripple Fractional-Slot PM-Motors," pp. 144–148, 2005.

[11] S. Wahsh and A. Elwer, "Improved performance of permanent magnet synchronous motor by using particle swarm optimization techniques," *2007 IEEE International Conference on Robotics and Biomimetics (ROBIO)*, pp. 2095–2100, 2007.

[12] Z. Li and A. Miotto, "Concentrated-winding fractional-slot synchronous surface PM motor design based on efficiency map for in-wheel application of electric vehicle," *2011 IEEE Vehicle Power and Propulsion Conference, VPPC 2011*, 2011.

[13] C. a. C. Coello, G. T. Pulido, and M. S. Lechuga, "Handling multiple objectives with particle swarm optimization," *Evolutionary Computation, IEEE Transactions on*, vol. 8, no. 3, pp. 256–279, 2004.

[14] M. van der Geest, H. Polinder, and J. a. Ferreira, "Optimization and comparison of electrical machines using particle swarm optimization," *XXth ICEM*, 2012.

[15] J. Pyrhönen, T. Jokinen, and V. Hrabovcová, *Design of Rotating Electrical Machines*. 2008.

[16] N. Bianchi and M. Dai Pre, "Use of the star of slots in designing fractional-slot single-layer synchronous motors," *IEE Proceedings - Electric Power Applications*, vol. 153, no. 3, p. 459, 2006.

[17] K. J. Meessen, P. Thelin, J. Soulard, and E. a. Lomonova, "Inductance Calculations of Permanent-Magnet Synchronous Machines," *IEEE Transactions on Magnetics*, vol. 44, no. 10, pp. 2324–2331, 2008.

[18] M. Popescu, "Prediction of the electromagnetic torque in synchronous machines through Maxwell stress harmonic filter (HFT) method," *Electrical Engineering*, vol. 89, no. 2, pp. 117–125, 2006.

[19] A. Boglietti, A. Cavagnino, and D. Staton, "Determination of Critical Parameters in Electrical Machine Thermal Models," *IEEE Transactions on Industry Applications*, vol. 44, no. 4, pp. 1150–1159, 2008.

[20] Y. Duan and R. G. Harley, "A Novel Method for Multiobjective Design and Optimization of Three Phase Induction Machines," *IEEE Transactions on Industry Applications*, vol. 47, pp. 1707–1715, July 2011.